Phase noise in a Duffing oscillator induced by quantum turbulence

C. S. Barquist,[*] W. G. Jiang ⬤, K. Gunther, and Y. Lee[†]

Department of Physics, University of Florida, Gainesville, Florida 32611, USA

H. B. Chan

Department of Physics, Hong Kong University of Science and Technology, Clear Water Bay, Kowloon, Hong Kong

We report a comprehensive investigation of the effects of quantum turbulence and quantized vorticity in superfluid ^{4}He at ultralow temperatures on a nonlinear microelectromechanical systems (MEMS) resonator which is uniquely sensitive to fluctuations of quantum turbulence. We observe that the phase noise of the MEMS is significantly increased in the presence of turbulence, while the noise in the amplitude channel is negligible in comparison. We formulated a model based on a fluctuating number of vortices pinned on the device to explain the observed noise. We also present measurements of the noise statistics and power spectra, providing insight into the dissipation mechanism of vortices at the micrometer scale in the ultraquantum regime. The high degree of customizability of MEMS oscillators coupled with their sensitivity to a small number of vortices lays the foundation for a more complete understanding of the interaction between quantized vortices and oscillating structures, and also offers a window into the dynamics of single vortices and small-scale fluctuations of quantum turbulence.

I. INTRODUCTION

Quantum turbulence is found in macroscopically coherent quantum systems, such as superlfuid ^{4}He, ^{3}He, and Bose-Einstein condensates of ultracold gases [1–5]. Pure quantum turbulence differs from classical turbulence in that all of the circulation arises from microscopically thin quantized vortices. In superfluid ^{4}He, each vortex has identical circulation, $\kappa = h/m_4$ [6], and diameter $a_0 \simeq 10^{-10}$ m. Here, h is Planck's constant and m_4 is the mass of the helium atom. At finite temperatures in ^{4}He, quantum and classical turbulence can coexist giving rise to a new coupled turbulent flow [7–9]. Despite the different physical manifestation of quantum turbulence, it is remarkably similar to classical turbulence. For example, the decay rate of turbulent energy was found to have the same time dependence as predicted by the classical Kolmogorov-Ohbukov theory in both helium superfluids [10–15], and the ubiquitous $k^{-5/3}$ law and intermittency are present for turbulence in ^{4}He [16].

The similarities to classical turbulence arise from the polarization of quantized vortices, which allows for bundles of vortices to mimic classical vortices on scales larger than the average intervortex distance, $\ell = L^{-1/2}$, where L measures vortex line length per unit volume [17]. In this way, pure superfluid turbulence can behave quasiclassically [18]. This similarity stops at scales close to ℓ, where the individual nature of the quantized vortices is dominant.

In the ultralow temperature regime, conventional viscous damping is absent. However, quantum turbulence is observed to decay. Experiments [10–15,19] and simulations [17,20–24] have demonstrated that turbulent energy is transferred to smaller scales through a process analogous to the Richardson cascade [25] in the quasiclassical regime. This process involves the breakup of bundles into smaller parts. At the resolution of individual vortices, this process must cease, and a new process should emerge. At this scale the energy is contained in perturbations of the vortex lines, and the energy is thought to flow to yet smaller scales through nonlinear interactions of these waves in a process called the Kelvin wave cascade. However, this process has not been directly observed, due to a lack of an appropriate experimental probe.

Recently, small oscillating objects, such as vibrating wires [10,11,26–50], tuning forks [51–64], microspheres [65–71], vibrating grids [44,72–77], and nanoelectromechanical system devices [78], have proven to be effective tools for investigating many properties of quantum turbulence in ^{4}He and ^{3}He over a wide temperature range. However, so far in ^{4}He, none have been successful at investigating the fluctuation spectrum of turbulent energy or vortex line density, L.

In this paper we present the measurement of turbulent fluctuations in superfluid ^{4}He at 10 mK, using a nonlinear microelectromechanical system (MEMS) oscillator for detection. Previously, similar MEMS resonators have been used to study superfluid [79–81] and normal fluid [82] ^{3}He, and turbulent damping in superfluid ^{4}He [83]. In this work, we use a quartz tuning fork (TF) to generate the turbulence. The turbulent fluctuations in the fluid are measured by their influence on the MEMS plate resonator. A simple diagram of
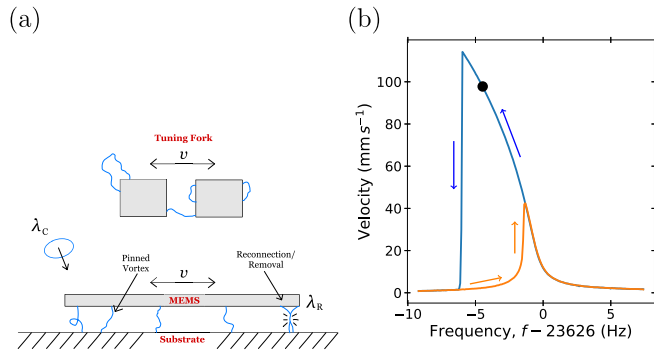
---

[*]cbarquist@ufl.edu

[†]ysl@ufl.edu

FIG. 1. (a) Schematic diagram of the experiment (not to scale). The TF sits $\simeq 3$ mm above the MEMS, while the MEMS sits 2 μm above the substrate. In turbulence, the MEMS captures vortices at a rate λ_C, which are removed at a rate λ_R (see text). (b) A plot of the velocity amplitude response of the MEMS in ^{4}He at 13 mK. The solid black dot represents where measurements of the noise are made.

the experiment can be seen in Fig. 1(a). The TF sits about 3 mm above the MEMS device, while the plate of the MEMS is suspended 2 μm above the substrate by four springs (not shown).

II. EXPERIMENTAL METHODS

A simple diagram of the experiment can be seen in Fig. 1(a). The TF sits about 3 mm above the MEMS device, while the plate of the MEMS is suspended 2 μm above the substrate by four springs (not shown). The MEMS device used in this study consists of a $125 \times 125 \times 2$ μm^3 center plate, four springs, and two pairs of capacitively coupled comb electrodes, one on either side of the device. The device is driven from one pair of electrodes and its displacement is measured as a change in the capacitance on the other pair. The same springs which suspend the device also provide the restoring force. The TF used in this study has two tines of dimension $100 \times 230 \times 2360$ μm^3. The TF is single crystal quartz and is actuated piezoelectrically. When driven, the tines oscillate in antiphase with their velocity directed parallel to the velocity of the MEMS. Only the fundamental mode, $f = 32\,768$ Hz, was used to generate turbulence.

The MEMS device has four main modes of oscillation: three which involve out-of-plane motion and change the thickness of the gap beneath the MEMS and one that does not. The modes are illustrated in Refs. [84,85]. In this work we only consider the shear mode, which leaves the gap size unchanged. The roughness of the surfaces has previously been characterized [84]. The average grain was found to be approximately 10 nm tall with a diameter of 140 nm.

While undergoing shear motion, the center-of-mass displacement, x, of the MEMS can be described by the following equation of motion:

$$\ddot{x} + 2\Gamma\dot{x} + \omega_0^2 x + \alpha_3 x^3 = g_0 \cos(\omega t), \qquad (1)$$

where Γ characterizes the damping on the device, $\omega_0/2\pi \simeq$ 23 kHz is the resonance frequency, α_3 is the strength of the conservative nonlinearity, $g_0 = f_0/m$, f_0 is the force on the device, and m is the mass of the device. The nonlinear restor-
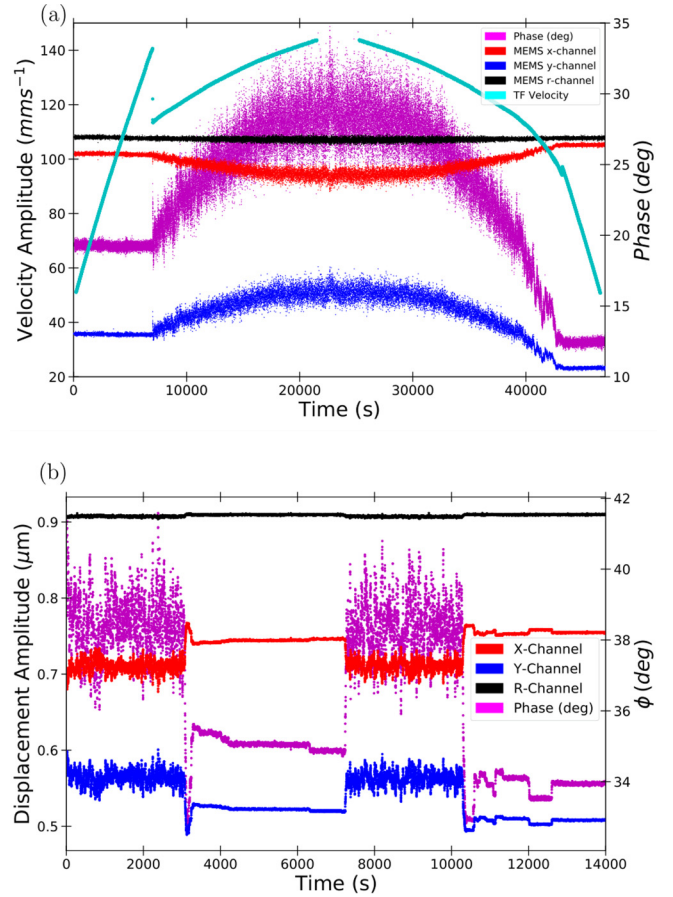

FIG. 2. (a) The amplitude (R-Channel), in-phase (X-Channel), out-of-phase (Y-Channel), and phase response of the MEMS to ramping of the TF velocity. (b) Time-dependent response of the MEMS device to a series of TF states [*on, off, on, off*] (see text).

ing force, α_3, arises from the nonlinear capacitive interaction of the electrodes. This term cannot be neglected as it is responsible for the response of the MEMS to parametric fluctuations [86].

Turbulence was generated by driving the TF on resonance to velocities exceeding the critical velocity, $v_c \simeq 140$ mm s^{-1}. Unlike in classical fluids, there is not a smooth transition to turbulent flow in superfluid ^{4}He. The transition from potential to turbulent flow of the TF can be seen in Fig. 2(a) as the discontinuous jump in TF velocity.

The measurements presented in this work were made in the ultralow temperature regime, 10 mK, where damping from the normal component of the fluid is negligible. In the absence of turbulence or remnant vortices, the damping is nearly equal to the damping measured in vacuum [83], and can be considered to only come from processes intrinsic to the polysilicon. Due to the extremely low damping, exciting the MEMS above the noise floor requires driving it into the nonlinear regime, where $\alpha_3 A_0^2 \simeq \Gamma\omega_0$ and A_0 is the amplitude on resonance. In this regime, the frequency response of the oscillator becomes hysteretic with two stable oscillation amplitudes around the resonance. A typical example of the MEMS frequency response is displayed in Fig. 1(b).

The mesaurement of noise in oscillating systems is usually made on resonance. However, in the nonlinear regime, fluctuations can induce a transition to the lower amplitude stable branch, where the MEMS loses its sensitivity. The strength of fluctuations needed to induce a transition is reduced as the device is driven close to resonance.

To measure the response of the MEMS device to turbulent fluctuations, we employed an open loop scheme where MEMS was driven at constant frequency, ω, and driving force amplitude, f_0. To begin the measurement, the MEMS was driven at a frequency above the bistable region and slowly reduced to the desired frequency, indicated by the black dot in Fig. 1(b). The output of the device was fed into a lock-in amplifier which was referenced at the driving frequency of the MEMS. In this way, we were able to directly measure the baseband fluctuations in the amplitude and phase. The lock-in time constant was chosen empirically to be short enough to ensure that the frequency spectrum of the noise was unaltered. The velocity of the TF was then adjusted to generate turbulence while the amplitude and phase of the MEMS were monitored. To get the frequency response, a discrete Fourier transform is performed on the time domain data.

III. RESULTS AND DISCUSSION

Time domain responses of the MEMS to turbulence can be seen in Fig. 2. Figure 2(b) shows the amplitude (R-Channel), in-phase (X-Channel), out-of-phase (Y-Channel), and phase response of the MEMS to a series of TF states, [*on, off, on, off*], where in the *on* state turbulence is being generated. The output of the MEMS is significantly noisier when the TF is generating turbulence. One can make a direct comparison between the quadrature components (X and Y) and the amplitude since they are plotted on the same scale. Notice that the noise in the quadrature components is more pronounced than the amplitude noise, indicating that the noise is predominantly in the phase. The amplitude noise is more than an order of magnitude smaller than the noise in the quadrature components. The mean signal change between the on and off states is also much larger for the quadrature components compared to the amplitude.

Figure 2(a) shows the response of the MEMS to a continuous ramp up of the TF drive amplitude followed by a continuous ramp down. At $t = 0$, the TF velocity is 51 mm s^{-1} and is in the potential flow regime. The TF remains in this regime until the velocity reaches 140 mm s^{-1}. The transition to the turbulent state is demarcated by the sudden decrease in the velocity, indicating an increase in damping. From there, the velocity continues to increase to 144 mm s^{-1}. The velocity is kept at this value for some time and then is reduced at the same rate. When the TF is in the potential flow regime, the response of the MEMS is unaffected by changes of the TF velocity. The excess noise in the MEMS only appears when the TF enters the turbulent regime. The amplitude of the noise increases as the velocity of the TF increases in the turbulent regime. This increase in noise occurs for all channels; however, it can be seen again that the amplitude noise is suppressed substantially compared to the quadrature noise. It is also noteworthy that the overall phase of oscillation is increased as the TF velocity is increased.
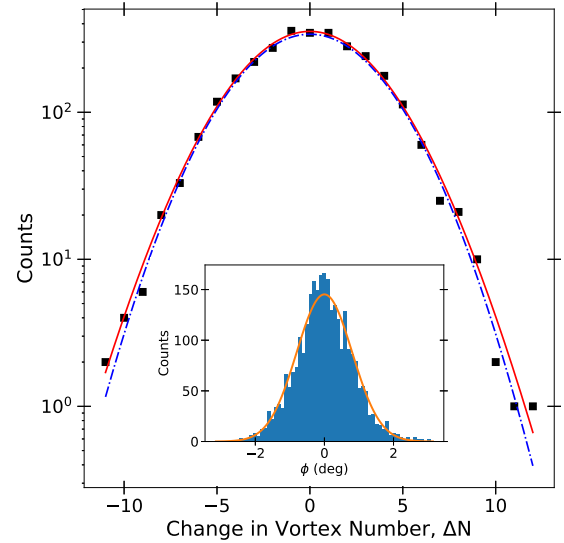

FIG. 3. Distribution of ΔN, the change in pinned vortices beneath the MEMS. The solid red line is a fit to the double Poisson process with $\lambda = 7.2 \pm 0.2$ s^{-1} and the dot-dashed blue line is a fit to a Gaussian distribution with $\sigma = 3.93$. Inset: Distributions of the noise amplitude for the phase noise. The solid curve is a Gaussian fit (see Table I).

The overall shift in phase and the predominance of phase noise in the presence of turbulence is due to the overall increase in damping and damping fluctuations. This can be understood from the arguments in Ref. [86]. The authors consider the effects of low-frequency parametric fluctuations to the response of a Duffing oscillator from the linear to strongly nonlinear regime over the whole resonance, showing that fluctuations in damping, Γ, manifest mainly as fluctuations in the quadrature components of the signal with relatively weaker fluctuations of the amplitude. On the other hand, for resonance frequency fluctuations, the relative strengths of the quadrature and amplitude noises are comparable in magnitude. Because we observe more than an order of magnitude difference in the relative amplitudes of the quadrature and amplitude noise, it can be concluded that the measured noise is caused predominantly by fluctuations in the damping. They also provide the following relationship between damping and phase changes:

$$\frac{d\phi}{d\Gamma} = \frac{1}{\Gamma} \frac{\cos\phi \sin\phi + 2A_0^2 \Pi/\Gamma \sin^4\phi}{1 + 2A_0^2 \Pi/\Gamma \cos\phi \sin^3\phi}, \qquad (2)$$

where $A_0^2 \Pi/\Gamma$ characterizes the degree of nonlinearity, and $\Pi = \frac{3}{8}\frac{\alpha_3}{\omega_0}$ determines the nonlinear frequency shift. For the MEMS, α_3 is negative and therefore Π is negative. From Eq. (2), the overall shift in the phase in the turbulent regime can be understood as an increase in the average damping experienced by the MEMS.

The statistical properties of the noise shown in Fig. 2(b) were calculated and are shown in Fig. 3. For this data set, the interval between successive measurements is 1.07 s, and the total time interval is 3106 s. The moments of these distributions are listed in Table I.

To explain the increased damping and excess noise in turbulence, we proposed a mechanism for damping based on the

TABLE I. Second, third, and fourth central moments of the time series shown in Fig. 2(b) and the distributions shown in Fig. 3. For reference, a pure Gaussian distribution has $\mu_3/\sigma^3 = 0$ and $\mu_4/\sigma^4 = 3$.

	σ^2	μ_3/σ^3	μ_4/σ^4
Phase	0.65 (deg^2)	0.13	3.34
Amplitude	64 (μV^2)	−0.15	3.10
X-Channel	6965 (μV^2)	−0.19	3.34
Y-Channel	9129 (μV^2)	0.07	3.34
δN	15.4	−0.02	3.03

interaction of the MEMS with vortices pinned between the movable plate and the substrate [83] [see Fig. 1(a)]. In this model the MEMS resonantly [83,87] pumps energy into the vortices pinned between the device and substrate. The energy flux into the vortices increases their length, which eventually leads to self-reconnection and ejection of vortex rings, carrying away the energy. The rate at which energy dissipated (damping) is proportional to the number of pinned vortices. In turbulence, the number of pinned vortices fluctuates giving rise to fluctuating damping experienced by the MEMS. The number of pinned vortices changes because vortex rings from the TF can be captured and existing pinned vortices can be removed through reconnection with other existing pinned vortices or vortex rings from the TF.

To relate changes in phase, $d\phi$, to changes in the pinned vortex number, dN, we use the following relationship $\frac{d\phi}{dN} = \frac{d\phi}{d\Gamma}\frac{d\Gamma}{dN}$. From this we can estimate the change in the number of vortices as

$$\Delta N = \frac{\Delta \phi}{(d\phi/d\Gamma)(d\Gamma/dN)}. \tag{3}$$

Here $\Delta\phi$ and ΔN are the change in phase and number of pinned vortices, respectively, between two different points in the time series. $d\Gamma/dN$ is a constant which depends on the static parameters of the MEMS device [88]. The distribution ΔN is shown in Fig. 3. The moments of the distribution are given in Table I. The dash-dotted line is a Gaussian with variance from Table I, and the solid red line is a fit to the data using the model described below.

To model the fluctuating number of pinned vortices, we consider that vortex rings ejected from the TF are captured randomly with a mean rate λ_C, and vortices are removed from beneath the MEMS randomly with a mean rate, λ_R. A cartoon of this process is shown in Fig. 1(a). In general the rate for capture and removal can vary independently. In steady state, when the average value of the damping is constant, the rates should be equal, $\lambda_C = \lambda_R = \lambda$. Assuming that the capture and removal events are random and uncorrelated, the probability of n capture or removal events in a duration T is then given by the Poisson distribution [39,89]

$$P(n; \lambda T) = \frac{e^{-\lambda T}(\lambda T)^n}{n!}. \tag{4}$$

The MEMS is not sensitive to individual capture or removal events. Rather, it is sensitive to the change in the total number of vortices within a measurement window. Therefore, we need to consider the probability of observing a change in vortex
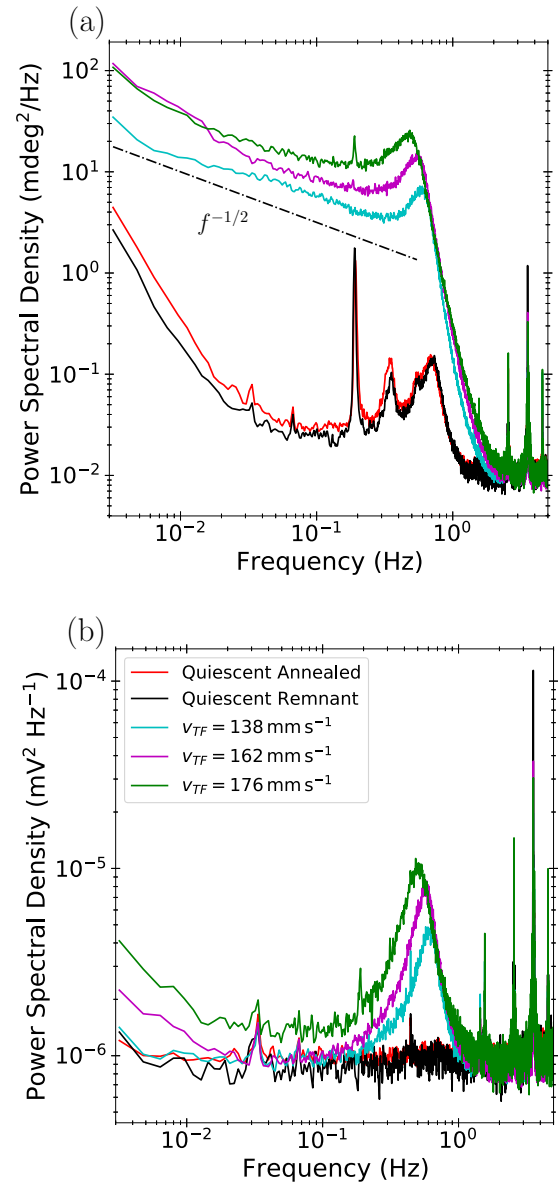

FIG. 4. Power spectrum of the MEMS signal in the presence and absence of turbulence. (a) Power spectrum of the phase noise. (b) Power spectrum of the amplitude noise.

number ΔN. Many different combinations of capture and removal events can result in a given ΔN. For example, observing $\Delta N = 1$ is consistent with one capture event and zero removals, while it is also consistent with two capture events and one removal. The distribution describing ΔN must contain a sum over all possible combinations. Then the distribution can be expressed as

$$P(\Delta N; \lambda T) = \sum_{a=0}^{\infty} P_C(\Delta N + a; \lambda T) P_R(a; \lambda T), \tag{5}$$

where P_C and P_R are the Poisson distributed probabilities of capture and removal, respectively. The sum over a accounts for the different combinations of removal and capture that lead to the same ΔN. A fit of the measured vortex fluctuations to Eq. (5) is presented in Fig. 3. From fitting to Eq. (5) we

determine that the capture and removal rates are $\lambda = 7.2 \pm 0.2 \text{ s}^{-1}$.

The power spectrum of the noise for several different TF velocities was also measured. Figure 4 shows the phase and amplitude power spectra for several different TF velocities including when the TF is off and not generating turbulence. When turbulence is not present, vortices can still remain pinned between the MEMS and the substrate and contribute to the damping of the MEMS [83,90]. These vortices can be removed from the device by driving the MEMS with a large amplitude. When the vortices have been removed we say the MEMS has been *annealed*.

In Fig. 4, the noise spectra in the absence of turbulence are shown with remnant vortices and after annealing in black and red, respectively. While the presence of the remnant vortices influence the damping on the device [83,90,91], their contribution to the noise is relatively small. This is consistent with the interpretation that the noise arises from the fluctuating number of pinned vortices in equilibrium with the surrounding vortex line density.

When turbulence is present, the amplitude and phase noise are both peaked around 0.7 Hz and roll off at higher frequencies. At lower frequencies the phase noise roughly follows an $f^{-1/2}$ power law, while the amplitude spectrum is flat and close to the noise floor. The noise in the quadrature channels (not shown) has an identical shape to the phase fluctuations, as the phase fluctuations drive the quadrature fluctuations [86]. The spikes at higher frequencies are likely resonances in the measurement circuit aliased to lower frequency and unassociated with the turbulence.

The $f^{-1/2}$ power spectrum of the phase noise must be inherited from the spectrum of the combined effects of the capture and removal processes. The power spectra of the phase fluctuations and the number of pinned vortices are related by

$$S_\phi(f) = \left(\frac{d\phi}{dN}\right)^2 S_N(f), \tag{6}$$

where $S(f)$ is the power spectrum and $d\phi/dN$ is defined above. In the low-frequency limit, $d\phi/dN$ is independent of frequency, and $S_N(f)$ and $S_\phi(f)$ have the same frequency dependence. If the capture and removal of vortices were independent of each other and the number of pinned vortices, the statistics and power spectra of the noise would be equivalent to that of a random walk, with the number of pinned vortices being analogous to the displacement. If this were true, $S_N(f) \sim f^{-2}$. From the power spectrum, the noise autocorrelation function can be determined using the Weriner-Kinchin theorem, which states that the two are Fourier transforms of each other. Using dimensional analysis, it can be determined that a $S_N(f) \sim f^{-1/2}$ corresponds to $\langle N(t)N(t-\tau)\rangle \sim \tau^{-1/2}$. Whereas, for a random walk $\langle N(t)N(t-\tau)\rangle \sim \tau^1$. The absence of long-time correlations likely arises from a limit in the number of vortices which can be pinned on the device [92] and a dependence of λ_R on the number of pinned vortices. While λ_R and λ_C must be equal in steady state, it is expected that λ_R will increase with increasing density of pinned vortices. This is because as the density increases the likelihood that two nearby vortices will collide, reconnect, and annihilate will increase. This mechanism will limit the growth of N, preventing a buildup of vortices, and attenuating long-time correlations.

IV. CONCLUSION

In summary, we have shown that our MEMS device is sensitive to turbulent fluctuations of superfluid ^{4}He in the ultralow temperature regime. The phase noise of the Duffing oscillator is enhanced by the presence of turbulence due to a fluctuating number of vortices pinned to the device. These fluctuations in pinned vortices are almost Gaussian and lack long-time correlations.

[1] R. J. Donnelly and C. E. Swanson, J. Fluid Mech. **173**, 387 (1986).

[2] W. Vinen and J. Niemela, J. Low Temp. Phys. **128**, 167 (2002).

[3] W. F. Vinen, J. Low Temp. Phys. **145**, 7 (2006).

[4] C. F. Barenghi, L. Skrbek, and K. R. Sreenivasan, Proc. Natl. Acad. Sci. USA **111**, 4647 (2014).

[5] M. C. Tsatsos, P. E. Tavares, A. Cidrim, A. R. Fritsch, M. A. Caracanhas, F. E. A. dos Santos, C. F. Barenghi, and V. S. Bagnato, Phys. Rep. **622**, 1 (2016).

[6] R. J. Donnelly, *Quantized Vortices in Helium II* (Cambridge University Press, Cambridge, UK, 2005).

[7] E. Varga, J. Gao, W. Guo, and L. Skrbek, Phys. Rev. Fluids **3**, 094601 (2018).

[8] S. Bao, W. Guo, V. S. L'vov, and A. Pomyalov, Phys. Rev. B **98**, 174509 (2018).

[9] J. Gao, E. Varga, W. Guo, and W. F. Vinen, Phys. Rev. B **96**, 094511 (2017).

[10] D. I. Bradley, D. O. Clubb, S. N. Fisher, A. M. Guénault, R. P. Haley, C. J. Matthews, G. R. Pickett, V. Tsepelin, and K. Zaki, Phys. Rev. Lett. **96**, 035301 (2006).

[11] D. I. Bradley, S. N. Fisher, A. M. Guénault, R. P. Haley, G. R. Pickett, D. Potts, and V. Tsepelin, Nat. Phys. **7**, 473 (2011).

[12] P. M. Walmsley, A. I. Golov, H. E. Hall, A. A. Levchenko, and W. F. Vinen, Phys. Rev. Lett. **99**, 265302 (2007).

[13] P. M. Walmsley and A. I. Golov, Phys. Rev. Lett. **100**, 245301 (2008).

[14] D. E. Zmeev, P. M. Walmsley, A. I. Golov, P. V. E. McClintock, S. N. Fisher, and W. F. Vinen, Phys. Rev. Lett. **115**, 155303 (2015).

[15] P. M. Walmsley and A. I. Golov, Phys. Rev. Lett. **118**, 134501 (2017).

[16] J. Maurer and P. Tabeling, Europhys. Lett. **43**, 29 (1998).

[17] A. W. Baggaley, C. F. Barenghi, A. Shukurov, and Y. A. Sergeev, Europhys. Lett. **98**, 26002 (2012).

[18] P. Walmsley, D. Zmeev, F. Pakpour, and A. Golov, Proc. Natl. Acad. Sci. USA **111**, 4691 (2014).

[19] L. Skrbek and K. R. Sreenivasan, Phys. Fluids **24**, 011301 (2012).

[20] M. Tsubota, T. Araki, and S. K. Nemirovskii, Phys. Rev. B **62**, 11751 (2000).

[21] M. Kobayashi and M. Tsubota, J. Phys. Soc. Jpn. **74**, 3248 (2005).

[22] C. F. Barenghi, Physica D (Amsterdam, Neth.) **237**, 2195 (2008).

[23] A. W. Baggaley, C. F. Barenghi, and Y. A. Sergeev, Phys. Rev. B **85**, 060501(R) (2012).

[24] N. Sasa, T. Kano, M. Machida, V. S. L'vov, O. Rudenko, and M. Tsubota, Phys. Rev. B **84**, 054525 (2011).

[25] U. Frisch, *Turbulence* (Cambridge University Press, Cambridge, UK, 1995).

[26] H. Yano, A. Handa, H. Nakagawa, K. Obara, O. Ishikawa, T. Hata, and M. Nakagawa, J. Low Temp. Phys. **138**, 561 (2005).

[27] H. Yano, A. Handa, H. Nakagawa, M. Nakagawa, K. Obara, O. Ishikawa, and T. Hata, J. Phys. Chem. Solids **66**, 1501 (2005).

[28] N. Hashimoto, R. Goto, H. Yano, K. Obara, O. Ishikawa, and T. Hata, Phys. Rev. B **76**, 020504(R) (2007).

[29] N. Hashimoto, A. Handa, M. Nakagawa, K. Obara, H. Yano, O. Ishikawa, and T. Hata, J. Low Temp. Phys. **148**, 299 (2007).

[30] H. Yano, N. Hashimoto, A. Handa, M. Nakagawa, K. Obara, O. Ishikawa, and T. Hata, Phys. Rev. B **75**, 012502 (2007).

[31] R. Goto, S. Fujiyama, H. Yano, Y. Nago, N. Hashimoto, K. Obara, O. Ishikawa, M. Tsubota, and T. Hata, Phys. Rev. Lett. **100**, 045301 (2008).

[32] H. Yano, N. Hashimoto, R. Goto, K. Obara, O. Ishikawa, and T. Hata, J. Low Temp. Phys. **150**, 410 (2008).

[33] H. Yano, T. Ogawa, A. Mori, Y. Miura, Y. Nago, K. Obara, O. Ishikawa, and T. Hata, J. Low Temp. Phys. **156**, 132 (2009).

[34] Y. Nago, T. Ogawa, A. Mori, Y. Miura, K. Obara, H. Yano, O. Ishikawa, and T. Hata, J. Low Temp. Phys. **158**, 443 (2010).

[35] Y. Nago, M. Inui, R. Kado, K. Obara, H. Yano, O. Ishikawa, and T. Hata, Phys. Rev. B **82**, 224511 (2010).

[36] H. Yano, Y. Nago, R. Goto, K. Obara, O. Ishikawa, and T. Hata, Phys. Rev. B **81**, 220507(R) (2010).

[37] Y. Nago, T. Ogawa, K. Obara, H. Yano, O. Ishikawa, and T. Hata, J. Low Temp. Phys. **162**, 322 (2011).

[38] Y. Nago, A. Nishijima, H. Kubo, T. Ogawa, K. Obara, H. Yano, O. Ishikawa, and T. Hata, Phys. Rev. B **87**, 024511 (2013).

[39] H. Yano, K. Sato, K. Hamazaki, R. Mushiake, K. Obara, and O. Ishikawa, J. Low Temp. Phys. **196**, 184 (2019).

[40] H. Kubo, Y. Nago, A. Nishijima, K. Obara, H. Yano, O. Ishikawa, and T. Hata, J. Low Temp. Phys. **171**, 466 (2013).

[41] S. Oda, Y. Wakasa, H. Kubo, K. Obara, H. Yano, O. Ishikawa, and T. Hata, J. Low Temp. Phys. **175**, 317 (2014).

[42] S. N. Fisher, A. J. Hale, A. M. Guénault, and G. R. Pickett, Phys. Rev. Lett. **86**, 244 (2001).

[43] D. I. Bradley, S. N. Fisher, A. M. Guénault, M. R. Lowe, G. R. Pickett, A. Rahm, and R. C. V. Whitehead, Phys. Rev. Lett. **93**, 235302 (2004).

[44] D. I. Bradley, D. O. Clubb, S. N. Fisher, A. M. Guénault, R. P. Haley, C. J. Matthews, G. R. Pickett, V. Tsepelin, and K. Zaki, Phys. Rev. Lett. **95**, 035302 (2005).

[45] D. I. Bradley, D. O. Clubb, S. N. Fisher, A. M. Guénault, R. Haley, C. J. Matthews, G. R. Pickett, and K. L. Zaki, J. Low Temp. Phys. **138**, 493 (2005).

[46] D. I. Bradley, S. N. Fisher, A. M. Guénault, R. P. Haley, S. O'Sullivan, G. R. Pickett, and V. Tsepelin, Phys. Rev. Lett. **101**, 065302 (2008).

[47] D. I. Bradley, S. N. Fisher, A. Guénault, R. P. Haley, V. Tsepelin, G. R. Pickett, and K. Zaki, J. Low Temp. Phys. **154**, 97 (2009).

[48] D. Bradley, S. Fisher, A. Ganshin, A. Guénault, R. Haley, M. Jackson, G. Pickett, and V. Tsepelin, J. Low Temp. Phys. **171**, 582 (2013).

[49] S. N. Fisher, M. J. Jackson, Y. A. Sergeev, and V. Tsepelin, Proc. Natl. Acad. Sci. USA **111**, 4659 (2014).

[50] D. I. Bradley, Phys. Rev. Lett. **84**, 1252 (2000).

[51] M. Blažková, M. Človečko, E. Gažo, L. Skrbek, and P. Skyba, J. Low Temp. Phys. **148**, 305 (2007).

[52] M. Blažková, D. Schmoranzer, and L. Skrbek, Phys. Rev. E **75**, 025302(R) (2007).

[53] M. Blažková, M. Človečko, V. Eltsov, E. Gažo, R. De Graaf, J. Hosio, M. Krusius, D. Schmoranzer, W. Schoepe, L. Skrbek *et al.*, J. Low Temp. Phys. **150**, 525 (2008).

[54] M. Blažková, D. Schmoranzer, L. Skrbek, and W. F. Vinen, Phys. Rev. B **79**, 054522 (2009).

[55] D. Bradley, M. Fear, S. Fisher, A. Guénault, R. Haley, C. Lawson, P. McClintock, G. Pickett, R. Schanen, V. Tsepelin *et al.*, J. Low Temp. Phys. **156**, 116 (2009).

[56] D. Bradley, P. Crookston, S. Fisher, A. Ganshin, A. Guénault, R. Haley, M. Jackson, G. Pickett, R. Schanen, and V. Tsepelin, J. Low Temp. Phys. **157**, 476 (2009).

[57] D. Garg, V. B. Efimov, M. Giltrow, P. V. E. McClintock, L. Skrbek, and W. F. Vinen, Phys. Rev. B **85**, 144518 (2012).

[58] S. L. Ahlstrom, D. I. Bradley, M. Človečko, S. N. Fisher, A. M. Guénault, E. A. Guise, R. P. Haley, O. Kolosov, P. V. E. McClintock, G. R. Pickett *et al.*, Phys. Rev. B **89**, 014515 (2014).

[59] D. I. Bradley, M. J. Fear, S. N. Fisher, A. M. Guénault, R. P. Haley, C. R. Lawson, G. R. Pickett, R. Schanen, V. Tsepelin, and L. A. Wheatland, Phys. Rev. B **89**, 214503 (2014).

[60] D. I. Bradley, R. P. Haley, S. Kafanov, M. Noble, G. R. Pickett, V. Tsepelin, J. Vonka, and T. Wilcox, J. Low Temp. Phys. **184**, 1080 (2016).

[61] D. Schmoranzer, M. J. Jackson, V. Tsepelin, M. Poole, A. J. Woods, M. Človečko, and L. Skrbek, Phys. Rev. B **94**, 214503 (2016).

[62] S. L. Ahlstrom, D. I. Bradley, S. N. Fisher, A. M. Guénault, E. A. Guise, R. P. Haley, S. Holt, O. Kolosov, P. V. E. McClintock, G. R. Pickett *et al.*, J. Low Temp. Phys. **175**, 725 (2014).

[63] D. Duda, M. LaMantia, and L. Skrbek, Phys. Rev. B **96**, 024519 (2017).

[64] I. A. Gritsenko, T. A. Dubchak, K. A. Mykhailenko, S. S. Sokolov, and G. A. Sheshin, Low Temp. Phys. **44**, 36 (2018).

[65] J. Jäger, B. Schuderer, and W. Schoepe, Phys. Rev. Lett. **74**, 566 (1995).

[66] J. Jäger, B. Schuderer, and W. Schoepe, Physica B (Amsterdam, Neth.) **210**, 201 (1995).

[67] J. Jäger and W. Schoepe, Czech. J. Phys. **46**, 79 (1996).

[68] W. Schoepe, J. Low Temp. Phys. **161**, 526 (2010).

[69] W. Schoepe, J. Low Temp. Phys. **173**, 170 (2013).

[70] W. Schoepe, R. Hänninen, and M. Niemetz, J. Low Temp. Phys. **178**, 383 (2015).

[71] M. Niemetz, H. Kerscher, and W. Schoepe, J. Low Temp. Phys. **126**, 287 (2002).

[72] W. Vinen, L. Skrbek, and H. Nichol, J. Low Temp. Phys. **135**, 423 (2004).

[73] H. A. Nichol, L. Skrbek, P. C. Hendry, and P. V. E. McClintock, Phys. Rev. E **70**, 056307 (2004).

[74] H. A. Nichol, L. Skrbek, P. C. Hendry, and P. V. E. McClintock, Phys. Rev. Lett. **92**, 244501 (2004).

[75] D. Charalambous, L. Skrbek, P. C. Hendry, P. V. E. McClintock, and W. F. Vinen, Phys. Rev. E **74**, 036307 (2006).

[76] V. B. Efimov, D. Garg, M. Giltrow, P. V. E. McClintock, L. Skrbek, and W. F. Vinen, J. Low Temp. Phys. **158**, 462 (2010).

[77] D. I. Bradley, S. N. Fisher, A. M. Guénault, R. P. Haley, M. Kumar, C. R. Lawson, R. Schanen, P. V. E. McClintock, L. Munday, G. R. Pickett *et al.*, Phys. Rev. B **85**, 224533 (2012).

[78] A. Guthrie, S. Kafanov, M. T. Noble, Y. A. Pashkin, G. R. Pickett, V. Tsepelin, A. A. Dorofeev, V. A. Krupenin, and D. E. Presnov, Nat. Commun. **12**, 2645 (2021).

[79] P. Zheng, W. G. Jiang, C. S. Barquist, Y. Lee, and H. B. Chan, Phys. Rev. Lett. **117**, 195301 (2016).

[80] P. Zheng, W. G. Jiang, C. S. Barquist, Y. Lee, and H. B. Chan, Phys. Rev. Lett. **118**, 065301 (2017).

[81] P. Zheng, W. G. Jiang, C. S. Barquist, Y. Lee, and H. B. Chan, J. Low Temp. Phys. **187**, 309 (2017).

[82] M. González, W. G. Jiang, P. Zheng, C. S. Barquist, H. B. Chan, and Y. Lee, Phys. Rev. B **94**, 014505 (2016).

[83] C. S. Barquist, W. G. Jiang, K. Gunther, N. Eng, Y. Lee, and H. B. Chan, Phys. Rev. B **101**, 174513 (2020).

[84] M. González, P. Zheng, E. Garcell, Y. Lee, and H. B. Chan, Rev. Sci. Instrum. **84**, 025003 (2013).

[85] C. S. Barquist, Design, development, fabrication, and measurement of micro-electromechanical oscillators for the study of quantum turbulence and other super fluid properties, Ph.D. thesis, University of Florida, 2020.

[86] C. Barquist, W. Jiang, K. Gunther, and Y. Lee, Physica D (Amsterdam, Neth.) **427**, 132999 (2021).

[87] The resonance frequency of the MEMS is closely matched to the frequency of a standing mode for a vortex pinned between the device and the substrate.

[88] See Supplemental Material at http://link.aps.org/supplemental/10.1103/PhysRevB.106.094502 for a calculation of $\frac{d\Gamma}{dN}$.

[89] T. Nakagawa, S. Inui, M. Tsubota, and H. Yano, Phys. Rev. B **101**, 184515 (2020).

[90] C. S. Barquist, W. G. Jiang, P. Zheng, Y. Lee, and H. B. Chan, J. Low Temp. Phys. **196**, 177 (2019).

[91] C. S. Barquist, W. G. Jiang, K. Gunther, Y. Lee, and H. B. Chan, J. Low Temp. Phys. **201**, 4 (2020).

[92] D. D. Awschalom and K. W. Schwarz, Phys. Rev. Lett. **52**, 49 (1984).